Mechanisms of light scattering from biological cells relevant to noninvasive optical-tissue diagnostics

Judith R. Mourant, James P. Freyer, Andreas H. Hielscher, Angelia A. Eick, Dan Shen, and Tamara M. Johnson

We have studied the optical properties of mammalian cell suspensions to provide a mechanistic basis for interpreting the optical properties of tissues *in vivo*. Measurements of the wavelength dependence of the reduced scattering coefficient and measurements of the phase function demonstrated that there is a distribution of scatterer sizes. The volumes of the scatterers are equivalent to those of spheres with diameters in the range between ~0.4 and 2.0 μm. Measurements of isolated organelles indicate that mitochondria and other similarly sized organelles are responsible for scattering at large angles, whereas nuclei are responsible for small-angle scattering. Therefore optical diagnostics are expected to be sensitive to organelle morphology but not directly to the size and shape of the cells.

OCIS codes: 170.3660, 170.4580, 170.6510, 170.4730, 170.5280, 170.1530.

1. Introduction

To develop optical techniques for tissue diagnostics and therapeutics it is necessary to understand the relationship between optical and biological properties of tissue. There are two principal components to the interaction of light with tissue, scattering and absorption. Both can provide important information about the physiological condition of the tissue. In this paper we focus on only one of these two kinds of interaction, the scattering properties of cells. In particular we address the relationship between scattering and cell morphology and the issue of what features of cells are responsible for light scattering.

A fundamental understanding of the origin of light scattering from biological cells is relevant to a number of noninvasive medical diagnostic techniques for cancer and for other tissue pathologies. For example, optical coherence tomography,[1] elastic-scattering spectroscopy,[2,3] and photon migration[4] are all techniques that are being developed for noninvasive optical diagnosis of tissue and that in some way rely on light scattering from tissue to generate the measured signal.

Candidates for scattering centers in mammalian cells are the cell itself, the nucleus, other organelles, and structures within organelles. Mammalian cells are typically of the order of 10–30 μm in diameter, with nuclei of the order of 3–10 μm in diameter.[5] Mitochondria are approximately 1–4 μm in length and approximately 0.3–0.7 μm in diameter.[6] Lysosomes and peroxisomes are roughly spherical in shape and approximately 0.2–0.5 μm in diameter.[5] Other organelles from which light may scatter are the Golgi apparatus and the endoplasmic reticulum, both of which have complicated shapes containing a large proportion of lipid membranes.

To address the issue of what cell features are responsible for light scattering we measured the wavelength dependence of the reduced scattering coefficient, $\mu_s'(\lambda)$, and the angular dependence of scattering, $P(\theta)$. We then used these measurements to deduce information about the size distribution of the scattering particles. To relate $P(\theta)$ and the wavelength dependence of $\mu_s'(\lambda)$ to the size of the scatterers, we determined relationships between these measures and scatterer size. These relationships were obtained by Mie theory calculations for both monodisperse and polydisperse solutions of particles. We found that g is sensitive to the largest particles in the distribution, whereas $\mu_s'(\lambda)$ is more

J. R. Mourant, A. H. Hielscher, A. A. Eick, and T. M. Johnson are with the Bioscience and Biotechnology Group, MS E535, Chemical Sciences and Technology Division, Los Alamos National Laboratory, Los Alamos, New Mexico 87545. J. P. Freyer and D. Shen are with the Molecular and Cell Biology Group, MS M888, Life Sciences Division, Los Alamos National Laboratory, Los Alamos, New Mexico 87545.

Received 19 December 1997; revised manuscript received 11 February 1998.

0003-6935/98/163586-08$15.00/0

sensitive to the average and smaller-sized particles in the size distribution. Information on the wavelength dependence of $\mu_s'(\lambda)$ was then combined with the $P(\theta)$ measurements to yield information about the distribution of scatterer sizes. This knowledge about the sizes of structures in the cell provides clues to what morphological features are responsible for light scattering. In addition, angular scattering distributions from organelles isolated from cells were measured. Combining the results of these measurements with the angular scattering distribution from cells, we obtained correlations between the direction of scattering and the size of particle that is scattering.

In Section 4 the results of our measurements are combined with the results of other researchers to summarize the present knowledge of the source of light scattering from mammalian cells. The relevance of scattering from cells to scattering from tissue and the implications for clinical measurements are also discussed. In addition, the measurements of $P(\theta)$ are compared with the Henyey–Greenstein function and with theoretical calculations of $P(\theta)$ performed by other researchers.

2. Methods

A. Calculations of $\mu_s'(\lambda)$ and g for Distributions of Particles

Scattering from individual spheres was calculated from Mie theory based on the code of Bohren and Hoffman.[7] For N types of particles we deduced (in accordance with Gelebart *et al.*[8]) that

$$\mu_s(\lambda) = \sum_{i=1}^{N} \mu_{s,i}(\lambda), \tag{1}$$

$$P(\theta, \lambda) = \frac{\sum_{i=1}^{N} P_i(\theta, \lambda)\mu_{s,i}(\lambda)}{\sum_{i=1}^{N} \mu_{s,i}(\lambda)}, \tag{2}$$

where $\mu_{s,i}(\lambda) = N_i C_i(\lambda)$, N_i is the number density of spheres of type i, and $C_i(\lambda)$ is the extinction cross section for spheres of type i calculated by Mie theory.[5] The reduced scattering coefficient, $\mu_s'(\lambda)$, and the anisotropy factor, $g(\lambda)$, can be calculated by the following two equations:

$$g(\lambda) = \int P(\theta, \lambda)\cos\theta \, d\Omega, \tag{3}$$

$$\mu_s' = \mu_s(\lambda)[1 - g(\lambda)]. \tag{4}$$

To approximate a continuous distribution for a discrete number of particle sizes we used a radius step size of 0.001 μm. Refractive indices of 1.4 and 1.35 for the scatterers and the media, respectively, were used for these calculations. These values yield a relative refractive index of 1.04, which is a reasonable approximation for scatterers in cells and tissue.[9,10]

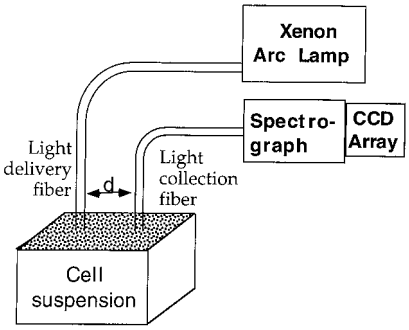

Fig. 1. Schematic of the experimental system used to measure elastic scatter as a function of both source–detector separation and wavelength. White light incident through the delivery fiber is scattered by the biological cell suspension. Some of this light is then detected by a collection fiber a distance d from the delivery fiber and dispersed onto a CCD array. The delivery fiber is 600 μm in diameter, and the collection fiber is 200 μm in diameter. Both fibers were set into pieces of black plastic in contact with the surface to match the boundary conditions near the fibers. The sample cell holding the cell suspension had a depth of 3 cm, a length of 3 cm, and a width of 1.9 cm.

B. Measurement of $\mu_s'(\lambda)$

Reduced scattering coefficients of suspensions of biological cells were determined as a function of wavelength. The data used for calculation of $\mu_s'(\lambda)$ were the elastic-scatter signals of the cell suspensions. These elastic-scatter signals were measured as a function of source detector separation, as shown schematically in Fig. 1. The reduced scattering coefficient, $\mu_s'(\lambda)$, can be calculated from these data by use of Eq. (5), which is derived based on the semi-infinite diffusion approximation to photon transport in a scattering medium[11,12]:

$$I(d) = \left\{ \mu_t' \left[\frac{\exp(-\mu_{\text{eff}} r_1)}{r_1} - \frac{\exp(-\mu_{\text{eff}} r_2)}{r_2} \right] + \frac{1}{\mu_t'} \left(\frac{1}{r_1} + \mu_{\text{eff}} \right) \frac{\exp(-\mu_{\text{eff}} r_1)}{r_1^2} + \left(\frac{1}{\mu_t'} + 2z_b \right) \left(\frac{1}{r_2} + \mu_{\text{eff}} \right) \frac{\exp(-\mu_{\text{eff}} r_2}{r_2^2} \right\}, \tag{5}$$

where

$$r_1 = [(1/\mu_t')^2 + d^2]^{1/2}, \qquad r_2 = \left[\left(\frac{1}{\mu_t'} + 2z_b \right)^2 + d^2 \right]^{1/2},$$

$$\mu_{\text{eff}} = \sqrt{\mu_a / D}, \qquad \mu_t' = \mu_s' + \mu_a,$$

$$D = \frac{1}{3(\mu_s' + \mu_a)}, \qquad z_b = 2AD.$$

A is a parameter that accounts for reflections at the surface of the cell suspension,[11] d is the separation between the source fiber and the detector fiber, and C is an overall amplitude factor. For this study a value of 1.1 was used for A, indicating a slight mismatch of boundary conditions. Changing A to a value of 1.0 does not change the results. C is the

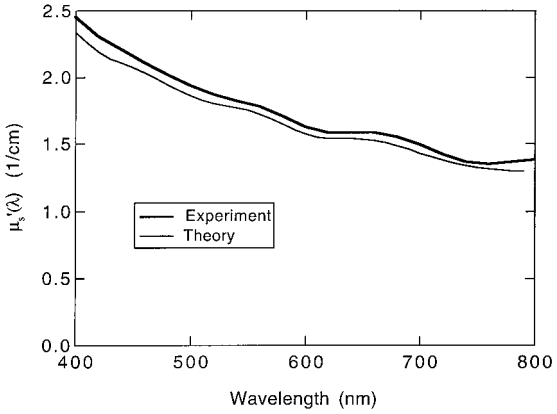

Fig. 2. Comparison of measurements and theory for $\mu_s'(\lambda)$ for 0.895-μm-diameter polystyrene spheres.

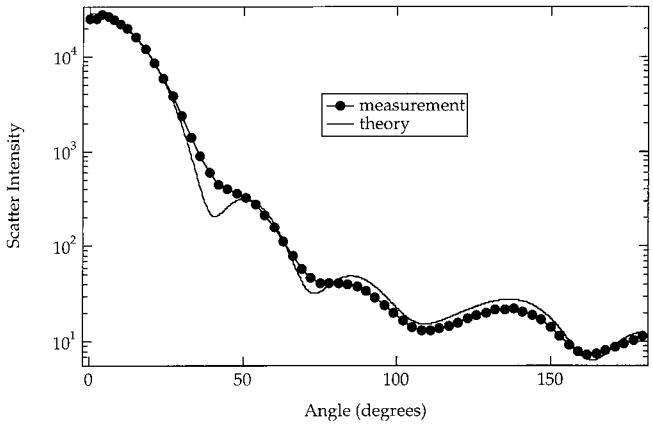

Fig. 4. Comparison of a measurement of $P(\theta)$ and a theoretical calculation of $P(\theta)$ for 0.895-μm-diameter polystyrene spheres. Both the measurements and the theoretical values are for unpolarized 632.8-nm incident light and unpolarized detection.

same for all wavelengths because we corrected the data for the wavelength dependence of the source, the fibers, and the detector by making a measurement of a spectrally flat diffuse reflector. To demonstrate the validity of this technique, in Fig. 2 we compare the measurement of $\mu_s'(\lambda)$ for a suspension of polystyrene spheres and Mie theory calculations of $\mu_s'(\lambda)$. The cells were measured at a concentration of $\sim 10^8$ cells/mL, which yielded values of $\mu_s'(\lambda)$ similar to that in Fig. 2.

C. Measurement of $P(\theta)$

We can obtain further information about the scattering centers by measuring the angular dependence of scattering, $P(\theta)$, with a goniometer. Measurements of cells and polystyrene spheres were made from 2° or 4° to 171° with an unpolarized He–Ne laser (632.8 nm). Measurements of organelles were made from 9° to 168°. In both cases we made extrapolations to 0° and 180° by linearly extrapolating $\log[P(\theta)]$. The goniometer system shown schematically in Fig. 3 had an angular resolution of 0.5° (set by the collection apertures), and measurements were made in steps of 2° at scatter angles less than 12° and in steps of 3° for larger angles. To measure the full range from 3° to 171° we used two cylindrically shaped quartz sample holders. One sample holder contained a black plastic backstop to reduce backscatter from the sample cell and was used for measuring angles greater than 12°. The other sample cell (with no backstop) was used for measuring scatter at angles less than 20°. Measurement of $P(\theta)$ requires a large dynamic range. Therefore optical-density filters were placed in front of the laser. The maximum power incident upon the sample was a few milliwatts. The concentration of cells was 10^5 cells/mL. This concentration was chosen so multiple scattering events would be rare enough not to affect the data. (We used the Poisson distribution to calculate the probability of multiple scattering events based on knowledge of μ_s.) Measurements made of suspensions diluted by a factor of 5 yielded no change in results, showing that multiple scattering effects were not an issue. Measurements took less than 30 min. The cells were assessed microscopically after the measurement, and the multiplicity (a measure of cell clumping) was determined and found to be ~1.1. To demonstrate the accuracy of the technique for determining $P(\theta)$ in Fig. 4 we compare measurements of polystyrene spheres and Mie theory calculations of $P(\theta)$ for the same polystyrene spheres. The reason for the discrepancy in the sharpness of the dips is unknown but could be the presence of nonspherical particles or a wider distribution of sphere sizes than stated by the manufacturer.

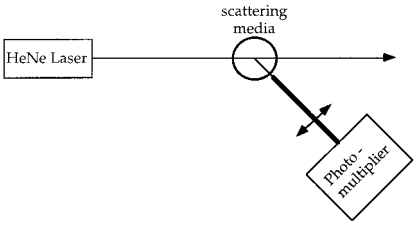

Fig. 3. Schematic of the goniometer system used for measuring $P(\theta)$. A He–Ne laser is incident upon a cylindrical sample cell containing a suspension of biological cells. The scattered light is measured as a function of angle by a photomultiplier tube, which is rotated around the sample cell. The thick black line represents a thin tube that is black on the inside and is critical for angular resolution and elimination of stray light. The intensity as a function of wavelength must be multiplied by the geometrical factor, $\cos\theta$, to account for the change in acceptance angle as the detector is rotated around the sample.

D. Biological Cell and Organelle Cell Suspensions

The mammalian cells used in this study were from an *in vitro* two-step tumorigenesis model.[13] Measurements were made of suspensions of both immortalized but nontumorigenic rat embryo fibroblast cells (M1) and a *ras*-transfected clone (MR1), which is highly tumorigenic. Cells were cultured as monolayers and prepared for analysis as described elsewhere.[14] For the optical measurements the cells

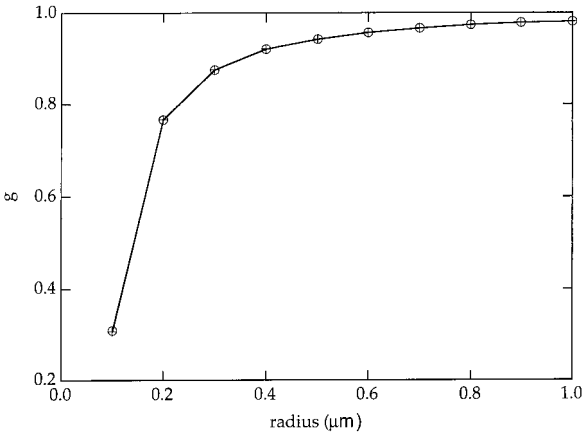

Fig. 5. Values of g for spheres calculated by Mie theory at 633 nm. Circles, sphere index of 1.4; crosses, sphere index of 1.41. In both cases the medium index was assumed to be 1.35.

were suspended in phosphate-buffered saline and kept on ice. These cells are spherical in shape when they are suspended in solution and have a volume of $\sim$1000 μm^3. Nuclei and mitochondria were isolated from MR1 cells by standard methods[15] and resuspended in mannitol sucrose buffer. The index of refraction of mannitol sucrose buffer (alone) was measured by the method of minimum deviation[16] and found to be 1.33–1.34.

3. Results

A. Relationship of g and $\mu_s'(\lambda)$ to Particle Size

Values of g obtained from Mie theory calculations for spheres of index 1.4 or 1.41 immersed in a medium of index 1.35 are plotted versus scatterer radius in Fig. 5. As the radius increases, so does the value of g. This relationship between g and mean radius is altered when there is a distribution of particle sizes. The value of g for a Gaussian distribution of sphere

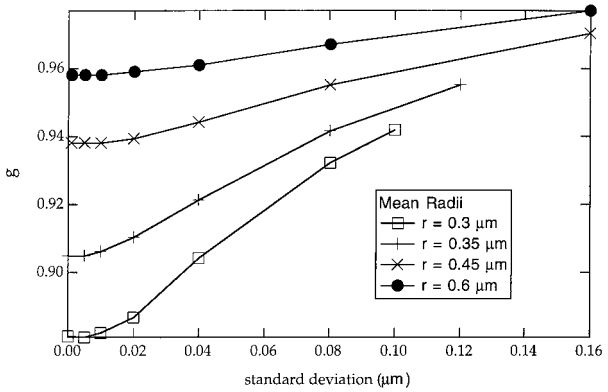

Fig. 6. Effect of the standard deviation on the value of g at λ = 633 nm for distributions of scatterer sizes. The distributions of scatterers were Gaussian with mean radii as shown. The standard deviation is stated on the x axis. (The Gaussian distributions of sphere sizes were truncated where the amplitude was 0.05 of the peak.) The refractive indices of the scatterer and the media were 1.4 and 1.35, respectively.

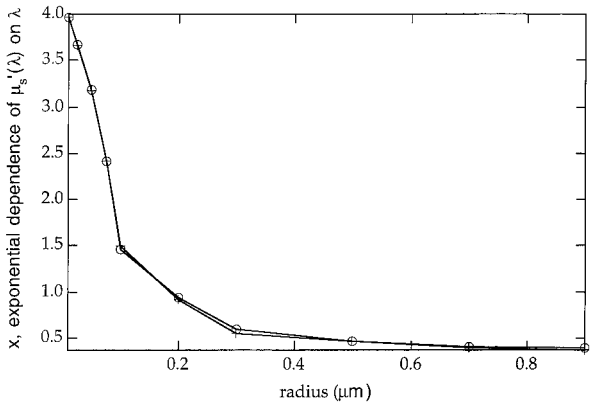

Fig. 7. Relationship between the radius of a scattering particle and the wavelength dependence of $\mu_s'(\lambda)$. The reduced scattering coefficient, $\mu_s'(\lambda)$, for narrow distributions of spheres sizes was fitted to $c\lambda^{-x}$. (The standard deviation was 0.005, except for the spheres with a radius of 0.01 μm, for which the standard deviation was 0.001.) The power-law dependence of $\mu_s'(\lambda)$ on wavelength, x, is plotted along the y axis. Circles, scatter index of 1.4; squares, scatter index of 1.45. In both cases the background medium had an index of 1.35.

sizes is not the same as the value of g for the mean of that distribution. Figure 6 demonstrates how the value of g depends on the standard deviation of a Gaussian distribution for spheres of four different radii. As the standard deviation increases (while the mean is held constant), the calculated value of g increases. The change is greatest for the smallest spheres, presumably because for a given increase in radius the increase in g is greater for smaller spheres (see Fig. 5).

Mourant *et al.* suggested a method for estimating the size of scatterers based on the wavelength dependence of $\mu_s'(\lambda)$.[17] Here we present the idea more clearly and expand on it by explicitly examining particle size distributions. The reduced scattering coefficient, $\mu_s'(\lambda)$, of suspensions of single-sized spheres was fitted to $c\lambda^{-x}$ over the wavelength range 400–800 nm. The dependence of radius on x, the power of λ, is shown in Fig. 7. There is no strong dependence on whether the index of the scatterer is 1.45 or 1.4 for a medium of index 1.35. For particles larger than 1 μm in radius the reduced scattering coefficient is proportional to $\lambda^{-0.37}$, as was shown by Graaff *et al.*[18] If the particles are smaller than 0.01 μm in radius then $\mu_s'(\lambda)$ will be proportional to $\lambda^{-4.0}$.

A distribution of scatterer sizes will alter the correlation between mean scatterer size and wavelength dependence. For a Gaussian distribution, the value of x depends on the standard deviation, as is shown in Fig. 8 for distributions with mean radii of 0.6, 0.45, 0.3, and 0.35 μm. As the distribution gets wider the value of x gets larger for a given radius. The effect is larger for smaller spheres, again because an increase in radius has a greater effect on x for smaller spheres (see Fig. 7). It is known from Fig. 7 that larger values of x correspond to smaller particles; therefore the wavelength dependence is more sensitive to the

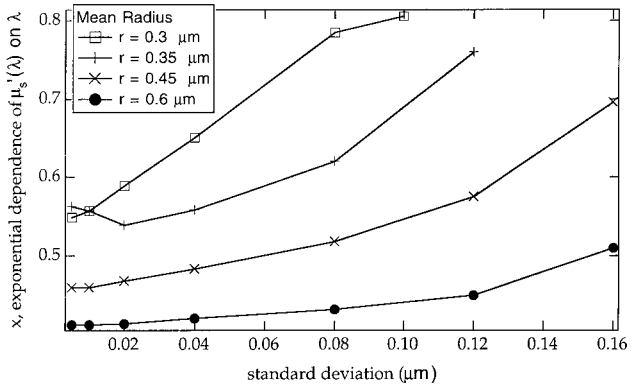

Fig. 8. Effect of the standard deviation on the power-law dependence of $\mu_s'(\lambda)$ on wavelength for distributions of scatterer sizes. The distributions of were Gaussian with mean radii as shown. The standard deviation is given on the x axis. (The Gaussian distributions of sphere sizes were truncated where the amplitude was 0.05 of the peak.) The refractive indices of the scatterer and the media were 1.4 and 1.35, respectively.

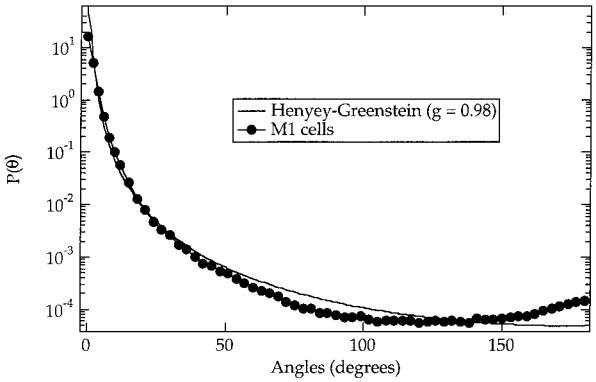

Fig. 10. Results of measuring the phase function of M1 cells at 633 nm. The values at 0° and above 171° were extrapolated as described in the text. A Henyey–Greenstein function with the same value of g as the phase function of the M1 cells is shown for comparison.

smaller particles than to the larger particles in the distribution. There is an anomally in Fig. 8 concerning the spheres of radius 0.35. For small values of the standard deviation the value of x is larger than expected. This is so because $\mu_s'(\lambda)$ is not a perfectly smooth function of λ for narrow distributions. Both $g(\lambda)$ and $\mu_s(\lambda)$ oscillate as a function of wavelength. These oscillations are significantly, but not completely, smoothed out for $\mu_s'(\lambda)$. (For a discussion of this point for spheres that are larger than a micrometer, see Graaff *et al.*[18]) For wider distributions $\mu_s'(\lambda)$ becomes a smoother function of wavelength.

B. Wavelength Dependence of $\mu_s'(\lambda)$

The wavelength dependence of $\mu_s'(\lambda)$ was measured for five sets of suspensions of M1 and MR1 cells. Figure 9 shows the results for one measurement of MR1 cells as well as for a fit to the function $c\lambda^{-x}$. The measurement of $\mu_s'(\lambda)$ is slightly affected by an absorption band at 560 nm that causes a small dip at that wavelength. Figure 9 shows fits both with and without the inclusion of data points near 562 nm. The fits are indistinguishable. On averaging all the data we found that $\mu_s'(\lambda)$ is proportional to $\lambda^{-1.0\pm(0.07)}$ for M1 cells and to $\lambda^{-0.95(\pm0.07)}$ for MR1 cells over the wavelength range 500–800 nm.

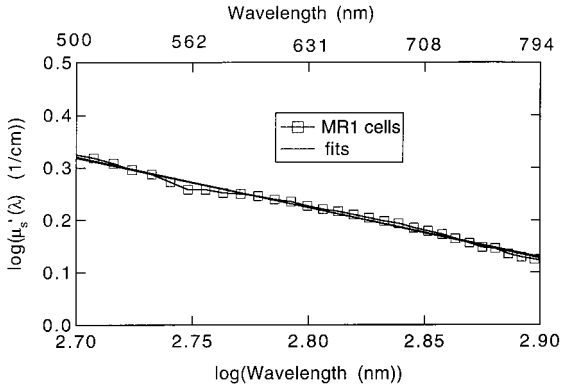

Fig. 9. Example of measurement of $\mu_s'(\lambda)$ for MR1 cells. The fits are to the function $c\lambda^{-x}$. One fit included points in the vicinity of 562 nm; the other did not.

C. Measurements of $P(\theta)$

An example of the angular scattering distribution of M1 cells is shown in Fig. 10. The results for MR1 cells are similar. Measurements were made of three separate pairs of suspensions of M1 and MR1 cells. The values of g calculated from the measurements were 0.980 ± 0.002 and 0.981 ± 0.005, respectively.

D. Estimation of Scatterer Size

From the wavelength dependence of $\mu_s'(\lambda)$ and Fig. 5 one might estimate that the size of the scatterers in the cells is approximately 0.2 μm. However, this estimation is valid only if there is a narrow distribution of scatterer sizes. Similarly, from the measured value of g, 0.98, and Fig. 7 one could estimate that the size of the scatterers is approximately 1.0 μm, although this estimation again holds only if there is narrow distribution of scatterer sizes. This discrepancy in estimated scatterer sizes based on assuming a monodisperse distribution indicates that there is a polydisperse distribution of sizes.

Our data are consistent with there being a broad distribution of scatterer sizes. Assume that there is a distribution of scatterers with a mean radius of 0.6 μm and a standard deviation of 0.16 μm. The measured value of g for this suspension will be (from Fig. 6) 0.98. The power-law dependence of $\mu_s'(\lambda)$ on λ will be 0.51 (from Fig. 8). On comparing this value with values of g and x for a monodisperse distribution of spheres of radius 0.6 μm ($g = 0.958$ and $x = 0.42$) we found that the g value of the polydisperse suspension is characteristic of a larger monodisperse suspension, whereas the wavelength dependence is indicative of a smaller monodisperse suspension. This is exactly what happened with our data. The measurement of g is sensitive to the largest scatter-

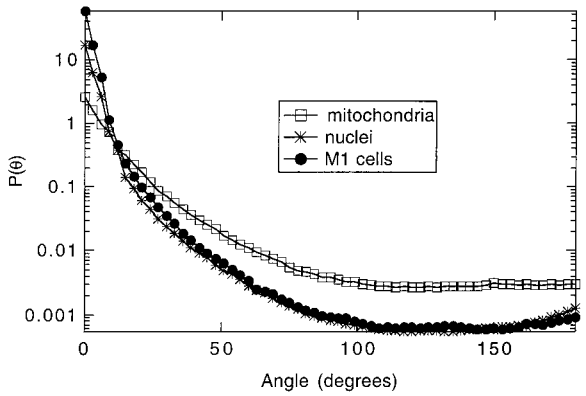

Fig. 11. Measured angular scattering distributions, $P(\theta)$, for cells, nuclei, and mitochondria. Values below 9° and above 168° were extrapolated as described in the text. All curves are normalized such that $\int P(\theta)d\Omega = 1$.

ers, and the measurement of $\mu_s'(\lambda)$ is sensitive to the average and smaller-sized particles. This analysis also shows that the distribution of scatterer sizes is quite wide, has a long tail, or is possibly bimodal, because the Gaussian distribution centered at 0.6 μm with a standard deviation of 0.16 μm was not sufficiently broad to have a steep enough wavelength dependence ($x = 0.51$ versus $x = 1.0$), although it did have a large enough value of g.

E. $P(\theta)$ Measurements of Nuclei and Mitochondria

Figure 11 compares the results of $P(\theta)$ measurements of nuclei and mitochondria with that of M1 cells. The scattering from the nuclei most closely resembles that from the cells. In particular the scattering at small angles is likely attributable to the nuclei, for if mitochondria alone were responsible for scattering the values of g would be much lower. The extrapolations of the organelle data below 9° (see Section 2) causes a small error. We examined this error with cell suspensions and found that the extrapolated data slightly underestimate forward scattering (g is underestimated by $<4\%$). This error is could account for the difference in forward scattering between the cells and the nuclei but is much smaller than the difference in forward scattering between the cells and the mitochondria.

4. Discussion and Analysis of Results

Our aim in this study was to measure the optical properties of biological cells and to elucidate information on what morphological features of the cells are relevant to light scattering. As we stated in Section 1, there are a wide variety of features in the cells that could be relevant to light scattering. Two basic approaches have been taken by researchers to examine the relationship between light scattering and structural properties of cells. One method is to measure scattering properties such as the phase function, the scattering coefficient, and the reduced scattering coefficient. The second is to examine the spatial variation of the refractive index.

The first approach, that of measuring optical properties, was taken by Beauvoit et al.[9,19,20] Reduced scattering and absorption coefficients of cells were measured at 780 nm. The reduced scattering coefficient of the yeast cells was shown to depend on the cell size.[19] Changes in nuclear ploidy and mitochondrial differentiation were also found to alter the reduced scattering coefficient of yeast cells, possibly through their effect on cell volume. In a study of scattering from hepatocyte cells and isolated mitochondria Beauvoit *et al*. found that mitochondria account for ~50% of the absorption of the liver and that "the origin of liver light scattering lies totally in its mitochondrial content."[9] Measurements of the reduced scattering coefficient at 780 nm of both neoplastic and nonneoplastic rodent tissues were performed with diffusive wave spectroscopy.[20] Light scattering was found to be generally proportional to mitochondrial content. The tumors and skeletal muscle all had low values of μ_s' and a small mitochondrial content, whereas the brain tissue had a larger μ_s' and a larger mitochondrial content. The liver, with the highest mitochondrial content, had the largest reduced scattering coefficient. Interestingly, if results for brain and liver tissue are disregarded, the correlation between mitochondrial content and reduced scattering coefficient is not as evident.

Nilsson *et al*.[21] measured $\mu_s'(\lambda)$ and g for liver tissue, using an integrating sphere. Estimates of scatterer size were then made based on the wavelength dependence of $\mu_s'(\lambda)$ and on the value of g. The authors did not consider the effects of a distribution of particle sizes. Scatterer radii were estimated to be 0.31 μm from the measurement of g and 0.29 μm from the wavelength dependence of $\mu_s'(\lambda)$. This size is consistent with the scatterers' being mitochondria. These results indicate that the scatterer distribution in liver tissue is much more homogeneous than in the fibroblast cells measured in the present study.

The second approach, that of measuring variations in refractive index, was taken by Schmitt and Kumar[22] and Beuthan *et al*.[23] Schmitt and Kumar found that the spectrum of index variations exhibits a power-law behavior for spatial frequencies from 0.5 to 5 μm^{-1}. In other words, they found evidence for a broad distribution of scatterers in cells with sizes ranging from 0.2 to 2 μm. Beuthan *et al*. concluded that only the nucleus and the membrane of the cell have a visibly different phase shift from the mean value of the cell and discussed membranes (both the cell membrane and those of organelles) as a source of scattering.

We can combine the results in this paper with those discussed above to describe the general nature of the relationship between light scattering from cells and morphological features. The size of the scattering centers varies in radius from less 0.2 μm to more than 1 μm. The organelle or cellular structure responsible for scattering is correlated with scatter angle. The cell itself is responsible for scattering at small angles, as is known from flow cytometry in which forward scatter (0.5°–1.5°) is regarded as an

estimate of the size of the a cell.[24] At slightly larger angles our data indicate that the nucleus is primarily responsible for scattering. Smaller organelles, such as mitochondria and lysosomes, are likely responsible for scattering at larger angles. Scattering from an organelle may be from the organelle itself as well as from features inside the organelle. A scatterer radius of 0.2 μm is very small for an organelle dimension and is more likely the size of a structural—possibly a membrane—feature of an organelle. The relative importance of different organelles still needs to be determined and will probably depend on cell type. The research of Beauvoit *et al*. provides strong evidence that mitochondria are primarily responsible for scattering from hepatocytes.[19] This result is corroborated by the research of Nilsson *et al*.,[21] which in addition provides evidence that the distribution of scatterer sizes is narrower in hepatocytes than in the fibroblasts studied in this paper. Hepatocytes are somewhat unusual cells in that mitochondria make up 28% of the cell volume.[25] In other types of cell, mitochondria are a significantly smaller fraction of the cell volume. For example, they are only 2.4% of the volume in human skin fibroblasts, whereas lysosomes are more than 2.7% of the volume.[26]

The measurements of optical properties of M1 and MR1 cells were made on cells in suspension. An important issue is then the relevance of the measurements to scattering from tissue. Tissue contains fibrous structures such as collagen and elastin as well as cells. However, many of the tissues for which optical diagnostics are being developed are epithelial (most cancer arises from epithelial tissue) and contain little fibrous structure.[27] Another issue of concern could be the fact that cells have a different shape in tissue than in suspension. The results described above show that scattering takes place from structures within the cells rather than from the surfaces of the cells; therefore the fact that the shapes of the cells in suspension are different from those in tissue is unlikely to change the scattering properties. We can also compare our values of μ_s' and g with those measured for tissue. Extrapolating our measurements of μ_s' (@600 nm) of cell suspensions to a cell density similar to that of tissue ($\sim 5 \times 10^8$ cells/mL), we found that μ_s' is ~ 8 cm^{-1}. This value is within the range of values of μ_s' that have been measured for tissue. There have also been a few measurements of $P(\theta)$ with which the results can be compared. Bovine muscle, pig brain, and white chicken muscle were found to have values of g in the range 0.94–0.965.[28] The value of g for human dermis has been measured to be 0.82,[29] and the phase functions of gray and white matter of the brain yielded values for g of 0.96 and 0.83, respectively.[30] These values are all somewhat lower than the value for g of 0.98 obtained for cells in this study.

The result that the majority of scattering is due to interactions of light with organelles has several implications for clinical measurements. Optical diagnostics may be sensitive to the micromorphology of the tissue, but they are not sensitive to the overall size (except indirectly through changes in number or size of organelles) or organization of the cells. This means that tissue diagnostics based on scattering changes should be based on changes in organelle structure and number. Another interesting consequence of a lack of sensitivity to cell size and shape is that optical scattering measurements of the bladder should not be sensitive to mild distension of the bladder because, although the cell shape changes,[25] organelles inside the cells are not affected. Small changes in optical probe pressure should also not have a serious effect on scattering properties. The different dependencies of small- and large-angle scattering on organelles also has interesting implications for clinical measurements. Possibly optical methods could be designed to be sensitive to particular organelles.

The measurements of phase function can be compared with the Henyey–Greenstein function often used to approximate the phase function of tissue as well as with the theoretical calculations of phase function of Dunn and Richards-Kortum.[31] Figure 10 compares the measured phase function with the Henyey–Greenstein function with the same value of g. The Henyey–Greenstein function significantly underestimates the amount of scattering at large angles. Dunn and Richards-Kortum calculated the phase function of single cells, using the finite-difference time-domain method. For a cell containing a nucleus and mitochondria they obtained a value of g of 0.992, which is significantly larger than the value of 0.98 measured in the present research. There is a also some difference in the shape of the phase functions. Our measured phase function shows a small increase in scattering with an angle starting at ~150 degrees, which is not present in the theoretical calculations.

5. Conclusions

The majority of scattering from a mammalian cell takes place from structures within the cell. There is a broad distribution of scatterer sizes in fibroblast cells. Measurements of the wavelength dependence of $\mu_s'(\lambda)$ are sensitive to the smaller-sized particles in a distribution and provide evidence for particles the size of a sphere with a 0.2-μm radius. Measurements of g are sensitive to the larger particles in a distribution and provide evidence for much larger particles (equivalent to a sphere with radius of 1.0 μm) that have a forward-directed scatter.

It is known from flow cytometry that scatter at the smallest angles is from the cell itself. Measurements of suspensions of nuclei and mitochondria demonstrate that the light scatter at small angles is most likely due to scattering from the larger particles such as nuclei. Scattering at larger angles could be due to smaller organelles and to structures within the organelles. Therefore we conclude that there is a correlation between the angle through which the light was scattered and the size of the scattering particle.

The result that the majority of scattering takes

place from organelles within the cell means that cell shape should have little effect on the scattering properties of the tissue. The independence of scattering properties from cell size has important consequences both in terms of the scientific basis for tissue diagnostics by means of light scattering and for the design of the optical measurement systems.

The Henyey–Greenstein function was shown to be a poor approximation of scattering from cells that underestimates scattering at large angles. The phase function calculated by Dunn and Richards-Kortum[31] for a cell containing nuclei and mitochondria was found to resemble the measured phase function more closely than the Henyey–Greenstein phase function did, although there are some discrepancies in shape and the calculated value of g was significantly higher than the measured value of g.

The authors thank Matt Gill, Melissa Muffoletto, and Tina Giovanielli for help in setting up the goniometer system and making preliminary measurements. We acknowledge helpful conversations with Irving Bigio concerning the measurement of refractive indices. This research was supported by National Institutes of Health grant 1R01CA71898.

References

1. G. J. Tearney, M. E. Brezinski, B. E. Bouma, S. E. Boppart, C. Pitris, J. F. Southern, and J. G. Fujimoto, "*In vivo* endoscopic optical biopsy with optical coherence tomography," Science **276,** 2037–2039 (1997).
2. J. R. Mourant, I. J. Bigio, J. Boyer, R. L. Conn, T. Johnson, and T. Shimada, "Spectroscopic diagnosis of bladder cancer with elastic light scattering," Lasers Surg. Med. **17,** 350–357 (1995).
3. J. R. Mourant, I. J. Bigio, J. Boyer, T. Johnson, and J. Lacey, "Detection of gastrointestinal cancer by elastic-scattering spectroscopy," J. Biomed. Opt. **1,** 192–199 (1996).
4. J. B. Fishkin, O. Coquoz, E. R. Anderson, M. Brenner, and B. J. Tromberg, "Frequency-domain photon migration measurements of normal and malignant tissue optical properties in a human subject," Appl. Opt. **36,** 10–20 (1997).
5. A. Alberts, D. Bray, J. Lewis, M. Raff, K. Roberts, and J. D. Watson, *Molecular Biology of the Cell* (Garland, New York, 1994), pp. 18–19.
6. G. E. Palade, "An electron microscope study of the mitochondrial structure," in *Mitochondria*, E. Sato, ed., Vol. 10 of Selected Papers in Biochemistry (University Park Press, Baltimore, Md., 1972), pp. 35–58.
7. C. F. Bohren and D. R. Hoffman, *Absorption and Scattering of Light by Small Particles* (Wiley, New York, 1983).
8. B. Gelebart, E. Tinet, J. M. Tualle, and S. Avrillier, "Phase function simulation in tissue phantoms: a fractal approach," Pure Appl. Opt. **5,** 377–388 (1996).
9. B. Beauvoit, T. Kitai, and B. Chance, "Contribution of the mitochondrial compartment to the optical properties of rat liver: a theoretical and practical approach," Biophys. J. **67,** 2501–2510 (1994).
10. J. M. Schmitt and A. Knuttel, "Model of optical coherence tomography of homogeneous tissue," J. Opt. Soc. Am. A **14,** 1231–1242 (1997).
11. T. J. Farrell, M. S. Patterson, and M. S. Patterson, "A diffusion theory model of spatially resolved, steady-state diffuse reflectance for the noninvasive determination of tissue optical properties *in vivo*," Med. Phys. **19,** 879–888 (1992).
12. R. C. Haskell, L. O. Svaasand, and T.-T. Tsay, "Boundary conditions for the diffusion equation in radiative transfer," J. Opt. Soc. Am. A **11,** 2727–2741 (1994).
13. L. A. Kunz-Schughart, A. Simm, and W. Mueller-Klieser, "Oncogene-associated transformation of rodent fibroblasts is accompanied by large morphological and metabolic changes," Oncol. Rep. **2,** 651–661 (1995).
14. K. E. A. LaRue, E. M. Bradbury, and J. P. Freyer, "Differential regulation of cyclin-dependent kinase inhibitors in monolayers and spheroid cultures of tumorigenic and nontumorigenic fibroblasts," Cancer Res. **58,** 1305–1314 (1998).
15. H. Lodish, D. Baltimore, A. Berk, S. L. Zipurssky, P. Matsudaira, and J. Darnell, *Molecular Cell Biology* (Freeman, New York, 1995), Chap. 5.
16. F. A. Jenkins and H. E. White, *Fundamentals of Optics*, 4th ed. (McGraw-Hill, New York, 1976), pp. 30–31.
17. J. R. Mourant, T. Fuselier, J. Boyer, T. M. Johnson, and I. J. Bigio, "Predictions and measurements of scattering and absorption over broad wavelength ranges in tissue phantoms," Appl. Opt. **36,** 949–957 (1997).
18. R. Graaff, J. G. Aarnoose, J. R. Zijp, P. M. A. Sloot, F. F. M. de Mul, J. Greve, and M. H. Koelink, "Reduced light-scattering properties for mixtures of spherical particles: a simple approximation derived from Mie calculations," Appl. Opt. **31,** 1370–1376 (1992).
19. B. Beauvoit, H. Liu, K. Kang, P. D. Kaplan, M. Miwa, and B. Chance, "Characterization of absorption and scattering properties of various yeast strains by time-resolved spectroscopy," Cell Biophys. **23,** 91–109 (1993).
20. B. Beauvoit, S. M. Evans, Y. W. Jenkins, E. Miller, and B. Chance, "Correlation between the light scattering and the mitochondrial content of normal and tissues and transplantable rodent tumors," Anal. Biochem. **226,** 167–174 (1995).
21. A. M. K. Nilsson, C. Sturesson, D. L. Liu, and S. Andersson-Engels, "Changes in spectral shape of tissue optical properties in conjunction with laser-induced thermotherapy," Appl. Opt. **37,** 1256–1267 (1998).
22. J. M. Schmitt and G. Kumar, "Turbulent nature of refractice-index variations in biological tissue," Opt. Lett. **21,** 1310–1312 (1996).
23. J. Beuthan, O. Minet, J. Helfmann, M. Herrig, and G. Muller, "The spatial variation of the refractive index in biological cells," Phys. Med. Biol. **41,** 369–382 (1996).
24. J. V. Watson, *Introduction to Flow Cytometry* (Cambridge U. Press, Cambridge, 1991), Chap. 10.
25. A. Bloin, R. P. Bolender, and E. R. Weibel, "Distribution of organelles and membranes between hepatocytes and nonhepatocytes in the rat liver parenchyma. A stereological study," J. Cell Biol. **72,** 441–455 (1977).
26. A. M. James, Y.-H. Wei, C.-Y. Pang, and M. P. Murphy, "Altered mitochondrial-function in fibroblasts containing Melas or Merrf mitochondrial-DNA mutations," Biochem J. **318,** 401–407 (1996).
27. L. C. Junquerira, J. Carneiro, and R. O. Kelley, *Basic Histology* (Appleton & Lange, Norwalk, Conn., 1992), pp. 66, 391.
28. S. T. Flock, B. C. Wilson, and M. S. Patterson, "Total attenuation and scattering phase functions of tissues and phantom materials at 633 nm," Med. Phys. **14,** 835–841 (1987).
29. S. L. Jacques, C. A. Alter, and S. A. Prahl, "Angular dependence of HeNe laser light scattering by dermis," Lasers Life Sci. **1,** 309–333 (1987).
30. P. van der Zee, M. Essenpreis, and D. T. Delpy, "Optical properties of brain tissue," in *Photon Migration and Imaging in Random Media and Tissues*, B. Chance, R. R. Alfano, and A. Katzir, eds., Proc. SPIE **1888,** 454–465 (1993).
31. A. Dunn and R. Richards-Kortum, "Three-dimensional computation of light scattering from cells," IEEE J. Sel. Topics Quantum Electron. **2,** 898–905 (1996).